Electron impact dissociative ionization of CO_2: Measurements with a focusing time-of-flight mass spectrometer

Cechan Tian and C. R. Vidal
Max-Planck-Institut für Extraterrestrische Physik, P.O. Box 1603, 85740 Garching, Germany

(Received 19 August 1997; accepted 9 October 1997)

For reliable cross section data a focusing time-of-flight mass spectrometer has been presented which collects all the ions produced by the electron impact dissociative ionization of molecules. The focusing characteristic of the mass spectrometer generates the ions close to the axis and focuses the energetic ions back to the detector. By observing the deflection curves we can measure the cross sections conclusively. The complete collection allows one to extract the initial kinetic energy distribution of the ions from the time-of-flight profiles of the mass peaks. As a first example we measured the cross sections of electron impact dissociative ionization of CO_2 for electron energies from threshold to 300 eV. The results agree very well with recent measurements of Straub *et al.* [J. Chem. Phys. **105**, 4015 (1996)], although previous data are in very poor agreement with each other. We measured the initial translational energy distribution of the fragment ions from the dissociative ionization of CO_2. With respect to the kinetic energy distribution of the ions we analyzed the techniques which make use of the quadrupole mass spectrometer. We discuss why the results from the quadrupole mass spectrometer underestimate the cross sections for the fragment ions. Finally we suggest to recheck the data from earlier quadrupole mass spectrometer measurements. © *1998 American Institute of Physics.* [S0021-9606(98)01803-0]

I. INTRODUCTION

Electron impact ionization of atoms and molecules is of fundamental importance in understanding the production of atomic and molecular ions and the extensive ion-molecule reactions in atmospheric science. It is also important in modeling plasma processes. To understand the electron impact ionization processes in space and in the laboratory, various reliable cross sections for the ionization and dissociative ionization are needed. This is why the ionization of atoms and molecules by electron impact has been investigated experimentally for about 60 years.[1,2] The experimental studies have been focused on either total[3,4] or partial cross section measurements.[5,6] Rapp and Englander-Golden measured the total cross sections of electron impact ionization of a variety of atoms and molecules in 1965.[3] Srivastava and co-workers developed a pulsed extraction technique and have made a series of measurements on the partial cross sections of atoms and molecules using a calibrated quadrupole mass spectrometer and a segmented time-of-flight (TOF) mass spectrometer in the past 10 years.[5,7,8] Recently, Straub *et al.* developed a short path length TOF technique and measured the absolute partial cross sections of the electron impact dissociative ionization of some atoms and molecules.[6,9–11] So far, the values for the total cross section from different measurements generally overlap with each other within the experimental errors and some reliable experimental values can be extracted. However, for partial cross sections, the agreement has only been achieved for rare-gas atoms and the parent ions of the dissociative ionization of a few molecules. The reported cross sections for the fragment ions produced in the dissociative ionization are confusing. For instance, in the dissociative ionization of CO_2, C^+ ions are produced, the very recent result of Straub *et al.*[6] for C^+ exceeds the result of Orient and Srivastava[5] by a factor of at least 4. This is so because during the ionization of the rare-gas atoms and direct ionization of molecules, the mass of the ejected electrons is much smaller than that of the ions, where the ions tend to keep their original translational energy and can more easily be collected. However, in the dissociative ionization of molecules, some more complicated processes may occur. If the electron energy lies between the first and second ionization limit, the fragment ions are produced by the dissociation of the molecular ions from the Franck-Condon region to the corresponding dissociation limit through the potential surfaces. If the electron energy is higher than the second ionization limit, the fragment ions can be produced by the dissociation of doubly or multiply ionized molecules. At even higher electron energies Auger processes may occur which also produce energetic fragment ions. The excess energy is determined by the potential difference between the region of the potential surface where the molecular ions have reached and the corresponding dissociation limit. The fragments share the excess energy according to their masses and the processes involved. Thus the fragment ions can achieve a kinetic energy of a few electron volts. The techniques applied so far have different limits in collecting energetic ions, which has been summarized in our previous work.[12] These energetic ions are not collected in some earlier measurements.

In order to get reliable cross sections for the electron impact dissociative ionization of molecules, we developed a focusing time-of-flight (FTOF) mass spectrometer in which the normal Wiley and McLaren[13] TOF mass spectrometer design has been modified. The ion source region is composed of extra shield plates to produce a focusing effect. Furthermore, the flight tube is segmented into two separate

tubes, with a high transmission mesh in-between. By applying an appropriate voltage the mesh behaves like a symmetric lens which focuses the diverging ion beam into the limited effective area of the detector. By observing the deflection curves we are able to say for sure whether we have collected all the ions. By analyzing the TOF profile of the mass peaks, we also get kinetic energy distributions of the fragment ions. This helps us to understand the process of the dissociative ionization and the reason why the results of some previous techniques are unreliable.

As the first example, we measured the cross sections of the electron impact dissociative ionization of CO_2. CO_2 is obviously very important in many environments. However, as pointed out in the very recent work of Straub *et al.*,[6] their results for CO_2 show very poor agreement with previous results. We will compare our results with existing values. We also report the result of the kinetic energy distribution of the fragment ions. With the kinetic energy measurement we are able to understand the disagreement in different measurement techniques. Finally some conclusive values will be given.

This paper is organized as follows. Section II introduces the experimental technique, which includes the pulsed electron gun, the FTOF mass spectrometer, the detection system, the measurement method of the kinetic energy distribution of the fragment ions, and the calibration procedure and the error estimate. In Section III the performance of the FTOF mass spectrometer is shown. In Section IV the results of the cross section values will be compared with other results. The kinetic energy measurements of the ions will be given as well. In Section V some of the existing techniques are discussed and the reasons why some previous techniques give unreliable results for the fragment ions. In Section VI some conclusions will be drawn.

II. EXPERIMENT

The experimental arrangement is shown in Fig. 1. A molecular beam and a pulsed (100 nsec) electron beam are crossed at right angles. About 100 nsec after the decay of the electron beam a pulsed extraction voltage (20 μ sec) is applied to the extraction mesh of the FTOF mass spectrometer. The ions produced by the ionization and the dissociative ionization of the molecules are extracted into the FTOF mass spectrometer. The axis of the FTOF mass spectrometer is perpendicular to both the electron and the molecular beams. The ions are accelerated to about 1.27 keV in the flight tubes and are focused by the focusing lens of the FTOF mass spectrometer. The bias voltage of the detector further accelerates the ions to 3 keV. The ions are detected by a three-stage microchannel plate (Hamamatsu F1208-31S with an effective diameter of 37 mm). The ion signal output from the microchannel plate is amplified by a fast amplifier (SR445) to about 0.7–1.2 V depending on the mass of the ions. A discriminator set at 0.3 V eliminates any noise, and the output is sent into a fast multichannel scaler (FAST 7886). The overall electronic repetition rate of the system is 1 kHz. For each point the counts are accumulated over 100 seconds. The

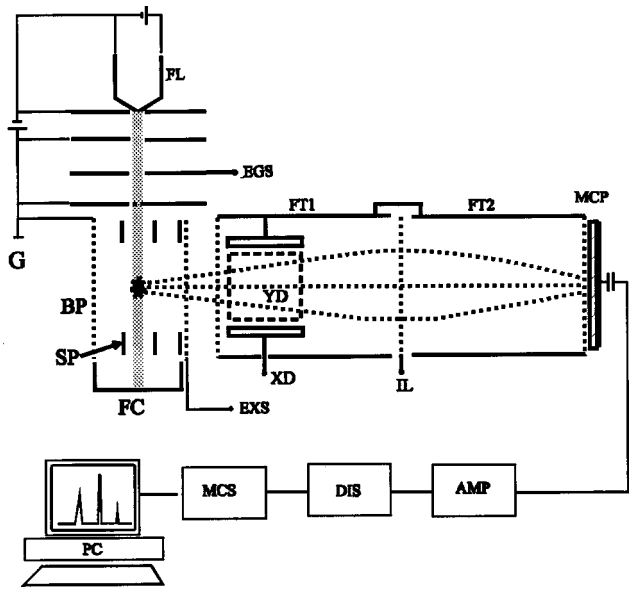

FIG. 1. Experimental arrangement of the TOF mass spectrometer. FL—filament; EGS—electron gun switch; FC—Faraday Cup; G—ground; BP—backing plate; SP—shield plate; EXS—ion extraction switch; YD—Y deflector; XD—X deflector; FT1—flight tube 1; FT2—flight tube 2; IL—ion lens; MCP—microchannel plate; AMP—amplifier; DIS—discriminator; MCS—mulitchannel scaler; PC—personal computer.

multichannel scaler counts the number of ions with a temporal resolution of 520 psec. During the accumulation the electron beam current and the density of the molecular beam are kept very low. The average maximum number of counts in each pulse is less than 1.5 avoiding any pile up.

A. Electron beam

The electron beam is produced by an electron gun, which is able to emit an electron beam current in excess of 20 μA at an electron energy exceeding 10 eV. The electron gun energy is calibrated to the ionization limit of Ar at 15.76 eV to ± 1 eV. The FWHM of the electron energy distribution is measured by observing the appearance potential of the ionization of Ar. The FWHM is about 0.6 eV, which actually corresponds to the voltage difference along the filament. A pulsed electric voltage of -1 kV is applied to the second lens of the electron gun, which pulses the electron beam at about 100 nsec. The electron beam is collected by a Faraday Cup, which shows that both the rise and fall times of the electron beam are less than 20 nsec. Measurements also show that the electron beam is completely collimated in a diameter of about 3 mm. During operation the average electron beam current is less than 100 pA.

B. Molecular beam

The gaseous samples are mixed with a reference gas (argon) inside a mixing bottle. The partial pressures of the reference gas and of the sample gas are measured by a MKS baratron manometer. During the measurements the pressure in the mixing bottle is kept constant to 1%. The gas enters the vacuum chamber through a leak valve and a long needle with a diameter of 0.3 mm. The divergence angle of the

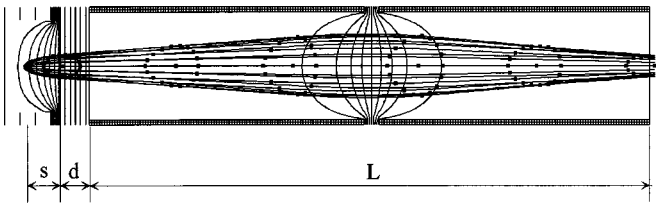

FIG. 2. Trajectories of the protons with 15 eV in the FTOF mass spectrometer. The extraction voltage is −600 V, the voltage on the flight tubes is −1.27 kV, and the voltage on the focusing mesh is −1.70 kV. The curves which cross the trajectories are the equipotential surfaces in steps of −100 V. The dot on each trajectory is the time clock, in steps of 100 nsec. The dot in the center of each curve is the time clock for 0 eV protons. The figure is cylindrically symmetric.

molecular beam has been determined to be less than 60 degrees. In order to make the interaction region as small as possible, the top of the needle is located at about 1 cm above the electron beam at the expense of a decreased mass resolution of the FTOF mass spectrometer. The interaction region of the electron beam and the molecular beam is estimated to be less than $4\times4\times12$ mm^3. The molecular density in the interaction region is about 10^{11} cm^{-3}. Without the operation of the molecular beam the background pressure in the vacuum chamber is below 1×10^{-7} mbar. With the operation of the molecular beam the background pressure increases to about 4×10^{-7} mbar.

C. The focusing time-of-flight mass spectrometer

The FTOF mass spectrometer is a modified Wiley-McLaren design, as shown in Figs. 1 and 2. The ion source region contains a backing mesh, three shield plates and an extraction mesh. The inner diameter of the shield plates is 3.6 cm. The backing plate and the three shield plates are grounded. As shown by the equipotential surfaces in Fig. 2, the extraction field thus also acts as a plane-convex lens to the ions. The ions which are located off-axis, or are produced with a big angle relative to the axis of the mass spectrometer, tend to be focused towards the axis. As a consequence, the divergence angle of the ion beam is smaller than that in a normal extraction field. This is the initial focusing region in the time-of-flight spectrometer. The distance between the extraction mesh and the backing mesh is 2.1 cm, and the length of the acceleration region is 1.2 cm. In the interaction region, the distance of the electron beam from the extraction mesh is about 1.3 cm. In this case calculations show that even if a proton is produced with an initial kinetic energy of 10 eV, it is still in the interaction region when the extraction voltage is applied. This guarantees that no ions escape in the first step.

Since the electron beam has a diameter of about 3 mm, the ions are produced in a relatively small region in the direction of the mass spectrometer and the space focusing condition required for a TOF mass spectrometer can still be fulfilled with the inhomogeneous extraction field, as will be shown later in the mass spectra.

The flight tube is separated into two tubes of identical length with a fine mesh in-between. The mesh is made of molybdenum wire of 20 μm in diameter. There are 6 wires per millimeter. The mesh between the two flight tubes acts as a focusing lens when the voltage applied to the mesh is about 1.3 times the voltage applied to the flight tubes. The equipotential curves behave as a symmetric spherical lens which makes the detector plane the image of the acceleration mesh. The inner diameter of the flight tube is 4 cm. The length of each flight tube is 10.5 cm. Experiments show that with this voltage the focusing mesh does not affect the mass resolution if we slightly increase the extraction voltage.

Typical trajectories of protons with 15 eV initial kinetic energy in the FTOF mass spectrometer are shown in Fig. 2. In the calculations with the SIMION software the extraction voltage is −600 V, the flight tube voltage is −1.27 kV, and the focusing voltage on the mesh is −1.7 kV. Initially the protons are assumed to be isotropically distributed over the full solid angle. The curves which cross the trajectories are the equipotential curves in steps of −100 V. The dot on each trajectory shows the time interval in steps of 100 nsec. The dots on the trajectories form a closed ringlike curve and the dot in the center of each curve corresponds to the clock for the proton starting with 0 eV which will be the center of the mass peak. Because of the initial backward and forward directions of the protons relative to the detector, the initial translational energy of the protons broadens the mass peak. From the trajectory calculations we see that without the focusing lens the ions will move in the direction of the flight tube 1 and some energetic ions may therefore escape detection. The focusing lens focuses the ions back to the detector.

Experimentally it is not enough to conclude that all the ions are collected if we just show the trajectory calculations. In the first flight tube we also have deflectors in both X and Y directions, where X corresponds to the direction of the electron beam, and Y corresponds to that of the molecular beam. If we change the deflection voltage, we are able to observe a constant count rate from the detector; this means that the diameter of the ion beam is smaller than the effective area of the detector. Hence we make sure that all the ions are collected by the detector.

Figure 2 shows that the initial translational energy broadens the mass peaks, from which we can extract the initial translational energy distribution of the ions. The flight time of the ions with mass m, charge q, and initial translational energy U_0 is described by[13]

$$t(s,U_0)=\sqrt{2m}\left(\frac{\sqrt{U_0+qE_s s}\pm\sqrt{U_0}}{qE_s}+\frac{\sqrt{U_0+U_s s+qE_a d}-\sqrt{U_0+U_s}}{qE_a}+\frac{L}{2}\frac{1}{\sqrt{U_0+U_s s+qE_a d}}\right), \tag{1}$$

where s is the distance from the electron beam to the extraction plate, and d is the length of the acceleration region. L is the total length of both flight tubes together. The $\pm$ sign corresponds to the initial velocity in backward or forward direction to the detector, respectively. E_s and E_a are the

electric fields in the source region and the acceleration region, respectively. U_s is the energy increase of the ions caused by the extraction field. The three terms of Eq. 1 describe the time-of-flight of the ions in the ion source region, in the acceleration region, and the flight tubes, respectively. As pointed out by Wiley and McLaren, the TOF mainly consists of the flight time in the flight tubes.[13] However, calculations show that the mass peak broadening originates mainly from the flight within the source region. In the present design E_s is not homogeneous. The time broadening is determined mostly by the local electric field in the interaction region. Later we will use the local field E_s to estimate the time-broadening of a mass peak. The presence of the focusing lens reduces the flight time by about 2%.

The initial kinetic energy distribution of the ions from the time-of-flight profile of a mass peak has been considered since 30 years.[14] If the initial kinetic energy of the ions has a very narrow distribution, Franklin *et al.* pointed out that the TOF profile of the mass peak will be nearly rectangular and the area of the rectangle is proportional to the total number of ions.[14] The position of the edges of the rectangle are determined by Eq. 1. However, in most cases the TOF spectrometer does not have the same collection efficiency for ions with different kinetic energies. If we simply analyze the TOF profile of a single mass peak, the result does not correspond to the initial kinetic energy distribution of the ions. Spinelli and co-workers simulated the ion trajectories in their TOF mass spectrometer and get the collection efficiency. They calibrate the TOF profile with the calculated collection efficiency.[15–17] Their collection efficiency decreases by two orders of magnitude for the ions with kinetic energies from 0.1 eV to 10 eV. In the present design all the ions are collected with the same efficiency which is only determined by the transmission of the meshes on the ion path. If we assume that the ions are generated isotropically, the initial kinetic energy distribution is $f(U)$ and the TOF profile on the rise side is described by

$$I(t_1-t_0)=\int_{U_1}^{\infty}\frac{1}{t_1-t_0}f(U)dU, \tag{2}$$

where t_0 is the time of the TOF mass peak. t_1 corresponds to the time edge of the ions with kinetic energy of U_1 in the forward direction, which is determined by Eq. 1 if the minus sign inside $\pm$ is taken. In the experiment we get $I(t_1\text{-}t_0)$, where the kinetic energy distribution can be obtained by

$$f(U_1)=-(t_1-t_0)\frac{d}{dt}I(t)\bigg|_{t=t_1-t_0}. \tag{3}$$

Here we note that the above equation will always vanish at $t_1=t_0$, which is not the case for the kinetic energy. We will use the TOF profile of the parent ions to determine the zero position of the kinetic energy and the resolution of the present experiment. This will be shown in detail in the kinetic energy analysis.

The presence of the focusing lens will distort the TOF profile. However, the simulation of the ion trajectories shows that if the initial kinetic energy of the ions is 6 eV, the distortion is less than 10%, and for 10 eV ions, the distortion is less than 20%. We use the leading edge of the TOF profile to obtain the kinetic energy distribution. The result should deviate from the real value just slightly in the high energy tail.

D. Normalization and error estimate

To get the absolute values of the cross sections, the counts of the ions, e.g. C^+ are normalized with respect to the reference gas, Ar, by the equation:

$$\sigma_{C^+}=\frac{I_{C^+}}{I_{Ar^+}}\frac{n_{Ar}}{n_{CO_2}}\sigma_{Ar^+}, \tag{4}$$

where I is the number of counts and n is the number density in the mixing bottle. Argon is used as the reference gas because its ionization cross section has been well determined. In this work, the very recent result of Straub *et al.* is used as the reference value.[9] Compared with the work of Straub *et al.*, the present work tends to measure the relative value of the cross sections. Since usually the cross sections for the parent ions from different measurements disagree very little, the determination of the relative cross sections is also important. Moreover, for inert gases like argon, very good agreement has been achieved,[9] which can therefore be used as the reference for the cross section measurements.

The total cross section is calculated from the contributions of the direct ionization and the dissociative ionization with respect to the weight of the fragment charges. The error in the cross sections of the fragment ions relative to the parent ions originates mainly from the data fluctuations in the measurement. Usually we make at least 5 independent measurements, and get the data fluctuations from these independent measurements. The electron current measurements, the electron gun reproducibility, and the pressure measurements do not contribute to the error of the relative measurements since all the ions are measured at the same time. The counts from the background gas are measured without the molecular beam and are usually less than 2% of the total count rate and are subtracted from the total count rate. The error in the cross sections of the fragments CO^+, O^+, and C^+ relative to that of the parent ions is estimated to be less than $\pm 6\%$. For the doubly charged fragments like CO_2^{2+}, O^{2+}, and C^{2+}, the error of the cross sections relative to that of the parent ions are estimated to be $\pm 10\%$. In determining the absolute cross sections, the error of the partial pressure measurements (less than $\pm 5\%$), the uncertainly of the cross sections of the reference gas ($\pm 3.6\%$) will contribute additionally. The general error for the cross sections of CO^+, O^+, and C^+ is expected to be less than $\pm 10\%$. For doubly charged ions, the error is expected to be less than $\pm 15\%$.

III. FTOF MASS SPECTROMETER PERFORMANCE

A typical mass spectrum of the mixture of Ar with CO_2 is shown in Fig. 3. For clarity the counts of C^{2+} and O^{2+} are multiplied by 500. We can see that all the ions are well resolved. The shape of each TOF mass peak will be

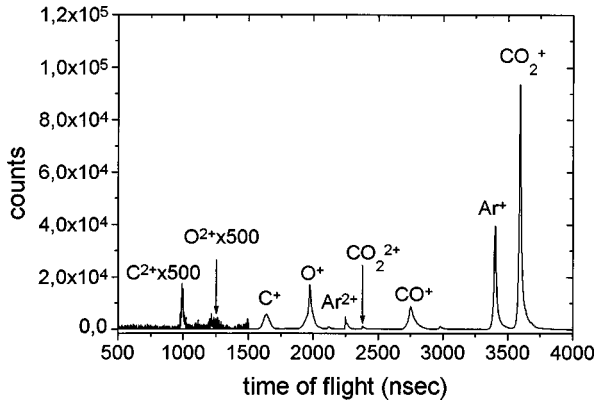

FIG. 3. A typical mass spectrum of the mixture of Ar with CO_2 . The counts of O^{2+} and C^{2+} are multiplied by a factor of 500.

used later to interpret the kinetic energy distribution of the ions. In order to make sure that all the ions are collected at the detector, we adjusted the voltages on the *X* and *Y* deflectors and observed the deflection curves. The ion counts as a function of the *X* and *Y* deflection voltages at the electron energy of 200 eV are shown in Fig. 4. The arrow in these figures indicates the voltage on the flight tube, −1.27 kV. The voltage on the mesh is −1.7 kV. The counts of CO_2^{2+} are multiplied by a factor of 10, whereas the counts of O^{2+} and C^{2+} are multiplied by a factor of 100, respectively. For the reference ion, Ar^+ , and the parent ion, CO_2^+ , the counts stay constant while the *X* deflection voltage ranges from −1.1 to −1.5 kV. The *Y* deflection voltage ranges from −1.1 to −1.7 kV. The difference between the *X* and *Y* directions is caused by the different dimensions of the crossing volume between the electron and molecular beams. This is also shown by the steepness in the decrease of the ion counts at lower and higher deflection voltages. For O^+ , the count

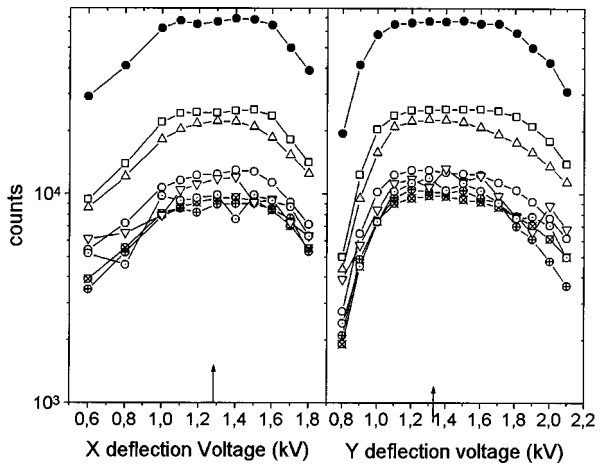

FIG. 4. The dependence of the ion count rates on the *X* and *Y* deflection voltages at an electron energy of 200 eV. (-●-) CO_2^+ , (-□-) Ar^+ , (-○-)CO^+, (-⊕-) $CO_2^{++}\times 10$, (-△-) O^+ , (-⊗-) C^+ , (-▽-)$O^{++}\times 100$, (-⊙-)$C^{++}\times 100$. When *X* (*Y*) deflection voltage is adjusted, the *Y* (*X*) deflection voltage is set to −1.27 kV which is identical to the flight tube voltage, as indicated by the arrows. The focusing mesh voltage is −1.70 kV. The count rates of CO_2^{2+} are multiplied by a factor of 10 and the count rates of O^{2+} and C^{2+} are multiplied by a factor of 100, respectively.

rates stay constant with the *X* and *Y* deflection voltages ranging from −1.2 to −1.4 kV. The O^+ ions have higher kinetic energies, so the ion beam has a much bigger divergence angle compared with that of the reference ions. The counts of C^+ and CO^+ are constant with *X* and *Y* deflection voltages in the range from −1.1 to −1.5 kV. The counts of CO_2^{2+} , O^{2+} and C^{2+} have higher fluctuations, but generally they are constant with the *X* and *Y* deflection voltages in the range from −1.2 to −1.5 kV. The flat tops on the deflection curves demonstrate experimentally that all the produced ions are collected to the detector.

When we set the voltage on the focusing lens identical to that on the flight tubes, the focusing mesh does not have a focusing effect. We measured the ion counts as a function of the deflection voltages. We find that the counts of Ar^+ and CO_2^+ are constant for the *Y* deflection voltage from −1.35 to −1.5 kV. At the flight tube voltage, −1.27 kV, the counts are much smaller. This is because in the experiment the interaction region is located off axis from the mass spectrometer, and the original molecules have a translational energy in this direction. Comparing the behaviors with and without the focusing lens, we conclude that with the focusing lens the tolerance of the detection system with respect to the initial position and the divergence angle of the ion beam is much bigger, which greatly helps the detector to collect all the ions.

When we set the *X* and *Y* deflection voltages both −1.27 kV identical to the flight tube voltage, and measure the ion counts as a function of the focusing voltage, since the interaction volume is located off-axis from the mass spectrometer, even the reference ions and the parent ions cannot be collected completely at the mesh voltage of −1.27 kV. As the mesh voltage increases, the ion counts also increase. At about −1.6 kV, all the count rates saturate, which further confirms that all the ions are collected at the detector. For the focusing voltage ranging from −1.3 kV to −1.6 kV, the count rates of different ions increase by different values. For instance, the enhancement of O^+ and CO^+ is much bigger than that of the reference ions. This suggests that if we measure the cross sections with a normal Wiley-McLaren design, we will possibly get smaller values for O^+ and CO^+ .

IV. RESULTS

A. Cross sections

The cross sections for the electron impact ionization and dissociative ionization of CO_2 are tabulated in Table I and plotted in Figs. 5–11, respectively. During the measurements, the *X* and *Y* deflection voltages are set to −1.27 kV, the focusing voltage is −1.7 kV. For comparison, all the existing data are also given in the figures, which contains the results of Straub *et al.*,[6] Freund *et al.*,[18] Krishnakumar,[19] Orient and Srivastava,[5] Märk and Hille,[20] Crowe and McConkey,[21] Adamczyk *et al.*[22] For the direct ionization (Fig. 5), there exists a variety of measurements and the results differ by about ±25% in amplitude. The results from a calibrated quadrupole mass spectrometer of Orient and Srivastava[5] and of Krishnakumar[19] lie about 25% above our

TABLE I. The ionization cross sections for electron impact on CO_2. The cross sections are in units of 10^{-16} cm^2.

Electron energy (eV)	CO_2^+	CO^+	CO_2^{2+}	O^+	C^+	O^{2+}	C^{2+}	total
300	1.76	0.309	0.0249	0.561	0.259	0.00326	0.00279	2.93
275	1.83	0.329	0.0265	0.599	0.273	0.00342	0.00306	3.07
250	1.93	0.355	0.0281	0.647	0.297	0.00343	0.00277	3.27
225	2.00	0.373	0.0293	0.675	0.311	0.00381	0.00280	3.40
200	2.06	0.395	0.0306	0.697	0.320	0.00302	0.00308	3.51
175	2.14	0.420	0.0335	0.728	0.340	0.00241	0.00228	3.68
150	2.19	0.434	0.0338	0.749	0.350	0.00210	0.00193	3.76
125	2.24	0.452	0.0343	0.741	0.345	0.00103	0.00134	3.82
110	2.31	0.472	0.0335	0.725	0.345	8.38E-4	9.30E-4	3.89
100	2.32	0.478	0.0313	0.705	0.335	6.72E-4	8.45E-4	3.87
90	2.35	0.481	0.0288	0.666	0.325	2.68E-4	5.05E-4	3.85
80	2.33	0.479	0.0254	0.611	0.304	1.05E-4	2.95E-4	3.75
70	2.30	0.460	0.0195	0.533	0.264			3.57
60	2.20	0.427	0.0113	0.428	0.214			3.28
50	2.06	0.377	0.0051	0.320	0.154			2.92
45	1.92	0.354	0.0029	0.267	0.112			2.66
40	1.800	0.318		0.216	0.068			2.41
35	1.68	0.253		0.175	0.035			2.15
30	1.42	0.137		0.116	0.006			1.70
25	1.00	0.044		0.064				1.18
20	0.449							0.45
17.5	0.08							0.08

values. Crowe and McConkey normalized their data to the total cross section measurements of Rapp and Englander-Golden.[3] Their results for the fragments tend to be smaller, hence their cross section for direct ionization is bigger. Our results agree very well with the absolute measurements of Straub *et al.*,[6] and lie in the middle of all the previous data, and overlap with all the data within the error bars.

For CO_2^{2+} (Fig. 6), the existing data originate only from Straub *et al.*,[6] and Märk and Hille.[20] Our results lie about 10% above those of Straub *et al.*, but overlap within the error limits. As for CO_2^+ (Fig. 5), the results of Märk and Hille lie below both the results of Straub *et al.* and ours. This might be caused by a systematic error of their equipment.

As pointed out by Straub *et al.*, their results for CO^+, O^+, and C^+ lie well above the previous data.[6] The discrepancies are much bigger than the quoted errors by different authors. However, our CO^+ results (Fig. 7) lie about 15% above their results, and overlap with them within the error limits. The results from the quadrupole mass spectrometer of Orient and Srivastava lie below the data of Straub *et al.* and ours by at least a factor of 3. The data of Crowe and McConkey lie below the present result by a factor of 2. For O^+ (Fig. 8) and C^+ (Fig. 9), the present results show excellent agreement with the absolute measurements of Straub *et al.* The results for O^+ of Orient and Srivastava, and of Crowe and McConkey lie below our results by a factor 3 and 2, respectively; whereas for C^+, the results of Orient and

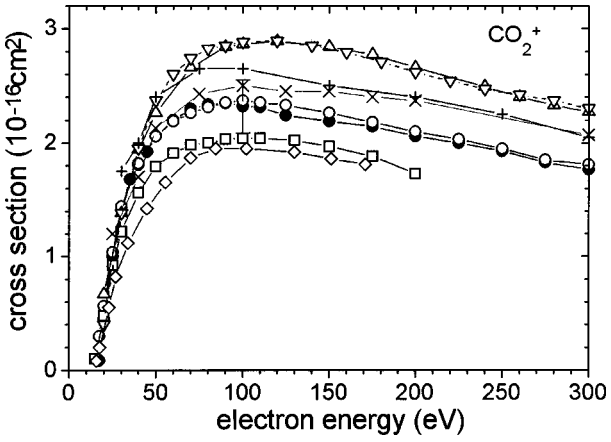

FIG. 5. The cross sections for ($CO_2 \rightarrow CO_2^+$. The present results (−●−) are compared with the results of Straub *et al.* (−○−) Ref. 6; Freund *et al.* (−□−) Ref. 18; Krishnakumar (−△−) Ref. 19; Orient and Srivastava (−▽−) Ref. 5; Märk and Hille (−◇−) Ref. 20; Crowe and McConkey (−+−) Ref. 21; and Adamczyk *et al.* (−×−) Ref. 22.

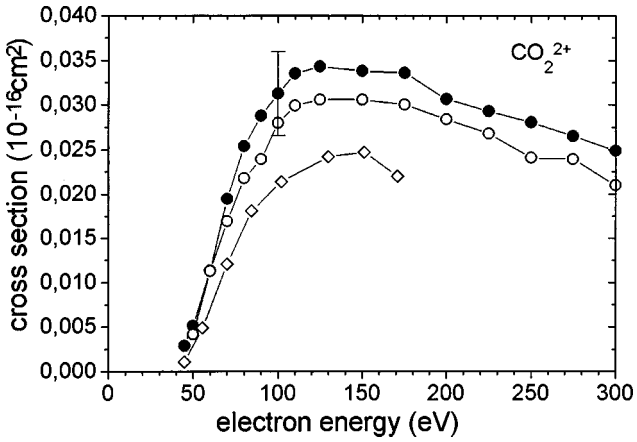

FIG. 6. The cross sections for CO2 → CO_2^{2+}. The present results (−●−) are compared with the results of Straub *et al.* (−○−) Ref. 6; Märk and Hille (−◇−) Ref. 20.

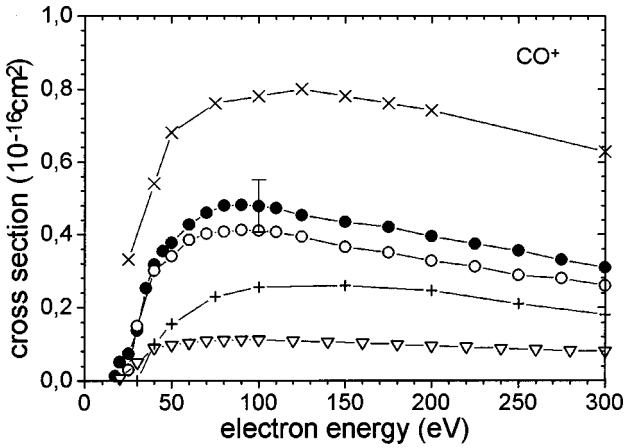

FIG. 7. The cross sections for $C_{2+} \rightarrow CO^+$. The present results (−●−) are compared with the results of Straub *et al.* (−○−) Ref. 6; Orient and Srivastava (−▽−) Ref. 5; Crowe and McConkey (−+−) Ref. 21; and Adamczyk *et al.* (−×−) Ref. 22.

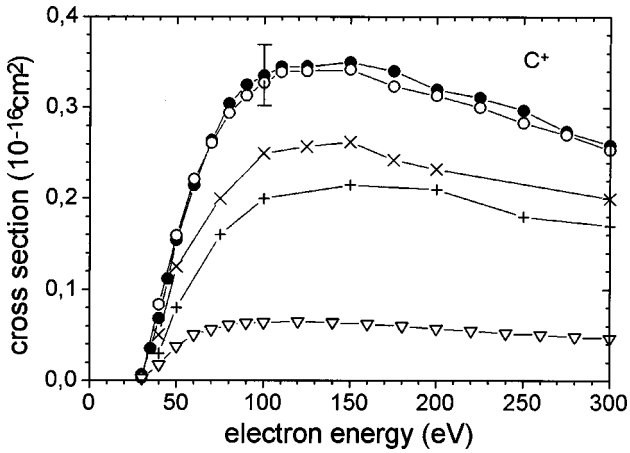

FIG. 9. The cross sections for $CO_2 \rightarrow C^+$. The present results (−●−) are compared with the results of Straub *et al.* (−○−) Ref. 6; Orient and Srivastava (−▽−) Ref. 5; Crowe and McConkey (−+−) Ref. 21; and Adamczyk *et al.* (−×−) Ref. 22.

Srivastava, and of Crowe and McConkey lie below our results by a factor 5 and 2, respectively.

For O^{2+} and C^{2+}, the only existing data are those of Straub *et al.* as shown in Figs. 10 and 11. Our results are in excellent agreement with those of Straub *et al.*, although the cross sections for these two fragments are three orders of magnitude below those of the parent ions. The appearance energy of O^{2+} is 75 ± 3 eV. The appearance potential of C^{2+} is 70 ± 3 eV, which agrees with the results of Velotta *et al.*[17]

For the ions O_2^+ and CO^{2+}, we agree with the maximum limit given by Straub *et al.*[6] At 200 eV, the cross section of O_2^+ is less than 10^{-19} cm^2. Straub *et al.* gave a maximum limit of less than 10^{-18} cm^2 for CO^{2+}. We believe that the cross section is even smaller. We estimated that it is smaller than 5×10^{-19} cm^2.

The total cross section of CO_2^+ is shown in Fig. 12 together with the results of Straub *et al.* and of Rapp and Englander-Golden. Our result agrees very well with that of Straub *et al.*, and lies about 10% above that of Rapp and Englander-Golden. However, the results overlap within the error limits.

B. Kinetic energy analysis

As seen in the last subsection, the discrepancy of the results of the parent ions in all the measurements lies generally within the error limits. However, the discrepancy for the fragment ions is usually larger than the mutual error limits, although careful calibration and normalization were made in all measurements. The difference is due to the much higher kinetic energy of the fragment ions. The measurement of the kinetic energy distribution of the fragment ions is thus useful for analyzing different measurement techniques and determine the ''final values'' of the cross sections.

The kinetic energy distribution of the fragments from the dissociation of CO_2 have recently been measured.[17,23,24] However, the results of the measurements show very poor agreement. In order to get the resolution of the present mea-

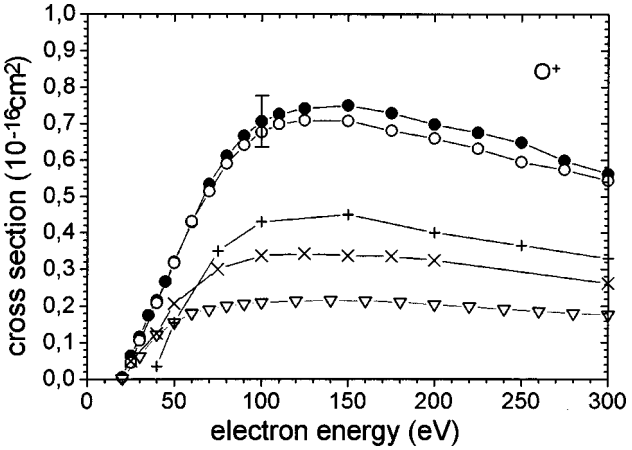

FIG. 8. The cross sections for $CO_2 \rightarrow O^+$. The present results (−●−) are compared with the results of Straub *et al.* (−○−) Ref. 6; Orient and Srivastava (−▽−) Ref. 5; Crowe and McConkey (−+−) Ref. 21; and Adamczyk *et al.* (−×−) Ref. 22.

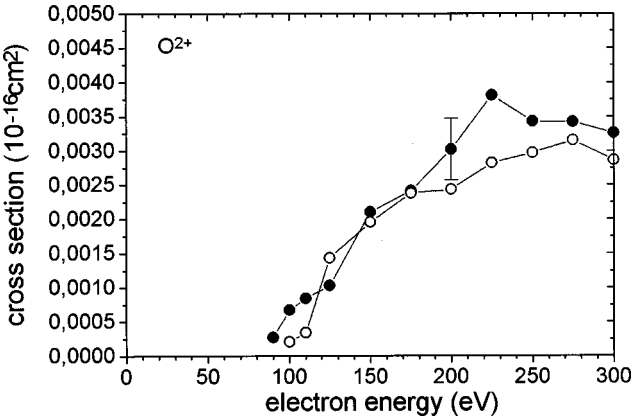

FIG. 10. The cross sections for $(CO_2 \rightarrow O^{2+}$. The present results (−●−) are compared with the results of Straub *et al.* (−○−) Ref. 6.

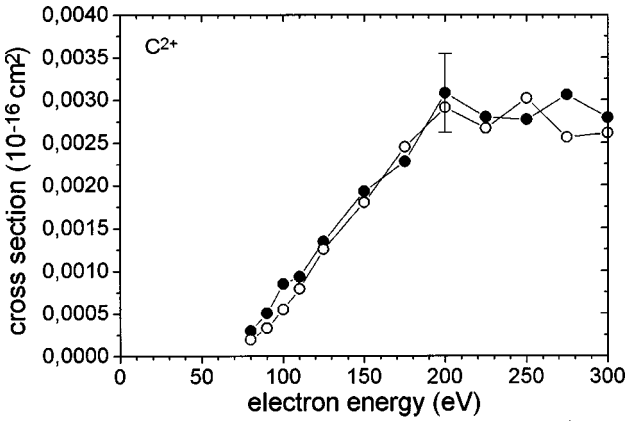

FIG. 11. The cross sections for $CO_2 \rightarrow C^{2+}$. The present results ($-\bullet-$) are compared with the results of Straub *et al.* ($-\circ-$) Ref. 6.

surements, we measured the TOF profile of the parent ions. The kinetic energy distribution of the parent ions is expected to be distributed in a narrow band near $U=0$. Since Eq. 3 always vanishes at the center of the mass peak, we applied Eq. 3 to the TOF profile of the parent ions, and define the maximum of the function as the zero position. The scale for the kinetic energy is determined by Eq. 1 with E_s as the local electric field at the interaction region. This may not be very accurate. However, we expect that the error is less than $\pm$ 20% . For the fragment ions the zero kinetic energy point is determined with respect to that of the parent ions, with regard to the $\sqrt{m}$ dependence on the TOF and its distributions. From the TOF profile of the parent ions we estimate that the resolution of the present measurement is better than 1 eV. Although the resolution is not very high, we collect all the ions without discrimination and hope that this measurement can provide an overview of the kinetic energy distribution of the fragment ions.

The derived kinetic energy distributions of C^+ at the electron energies of 200, 100, and 50 eV are shown in Fig. 13. The area of each curve is proportional to the corresponding cross sections. The TOF profiles of C^+ show no sharp

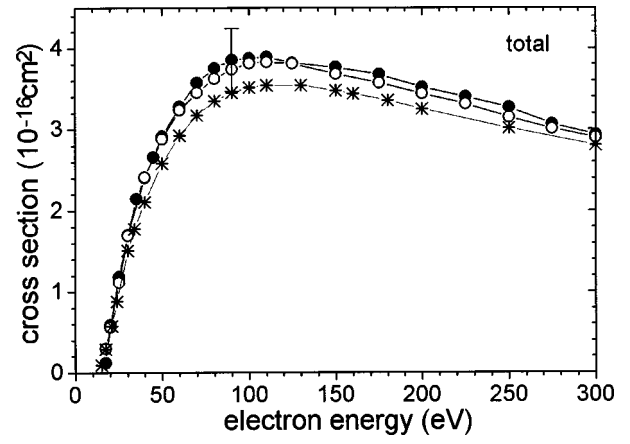

FIG. 12. The total cross sections of the electron impact dissociative ionization of CO_2. The present results ($-\bullet-$) are compared with the results of Straub *et al.* ($-\circ-$) Ref. 6; and Rapp and Englander-Golden (*) Ref. 3.

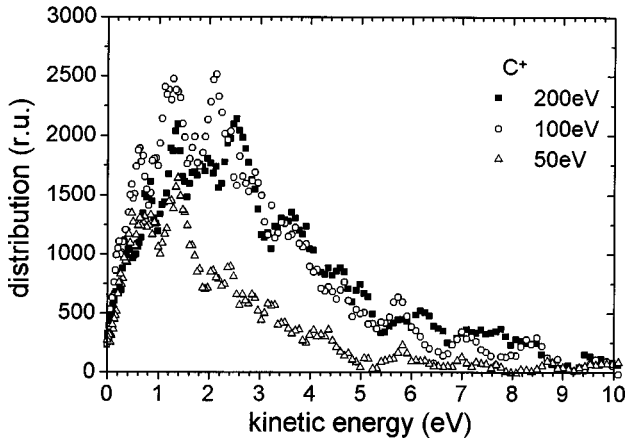

FIG. 13. The derived kinetic energy distributions of C^+ in relative units at the electron energies of 200, 100, 50 eV.

peak at the center and correspond to no clear maximum at 0 kinetic energy. Both Velotta *et al.*[17] and Locht and Davister[24] observed a maximum distribution at 0 kinetic energy. The measurement of Velotta *et al.* gives preference to the ions with 0 kinetic energy which may give false results. The measurement of Locht and Davister should discriminate to 0 kinetic energy, but they still observed a maximum at 0 kinetic energy. We do not understand the reason for this disagreement, but it is hard to believe that the present measurement discriminates to 0 kinetic energy ions. The maximum of the C^+ appears around 1–2 eV, which agrees with the plateau in the measurement of Velotta *et al.*

In strong contrast to the case of C^+, the TOF profiles of O^+ show a sharp peak at the center, which corresponds to a maximum distribution at 0 kinetic energy. The derived kinetic energy distribution is shown in Fig. 14. The maximum at 0 kinetic energy agrees with the results of Velotta *et al.* and Locht and Davister. The measurements of Zhukov *et al.*[23] discriminates against slow ions, but their results still show a slight maximum at 0 kinetic energy which also agrees with the present results. At electron energies around

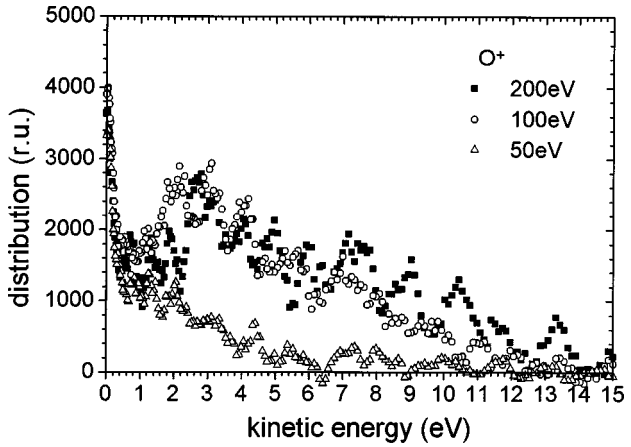

FIG. 14. The derived kinetic energy distributions of CO^+ in relative units at the electron energies of 200, 100, 50 eV.

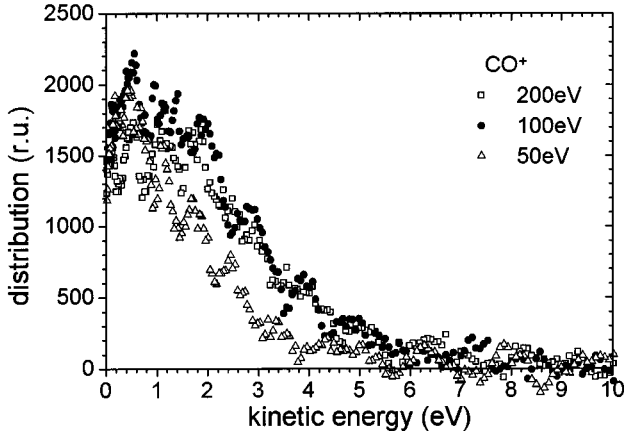

FIG. 15. The derived kinetic energy distributions of CO^+ in relative units at the electron energies of 200, 100, 50 eV.

100 eV, the present work, Zhukov *et al.*[23] and Velotta *et al.*[17] observed a maximum at 2–3 eV. However, this did not appear in the measurements of Locht and Davister.[24] The reason is possibly because the measurement of Locht and Davister discriminates against fast ions.[25]

The shape of the TOF profiles of CO^+ lies inbetween that of C^+ and O^+. The derived kinetic energy of CO^+ is shown in Fig. 15. There is a considerable number of ions distributed near the 0 kinetic energy. For electron energies around 100 eV there is a maximum at 1–2 eV. This agrees with the measurements of Zhukov *et al.*[23] and Velotta *et al.*[17] However, this maximum did not appear in the measurement of Locht and Davister.[24]

So far no kinetic energy measurements were reported for the doubly charged fragments of C^{2+} and O^{2+}. The TOF profiles of C^{2+} and O^{2+} at electron energy of 200 eV are shown in Fig. 16(a). The area of the TOF profiles is proportional to the cross section of the fragments. Clearly C^{2+} shows a much sharper TOF profile than O^{2+}. The derived kinetic energy distributions are shown in Fig. 16(b). The C^{2+} ions have a maximum near 0 eV, and decay towards higher kinetic energy. There is a long tail which extends to about 10 eV. The distribution of O^{2+}, however, is completely different. There is a maximum at about 1 eV. The distribution at the kinetic energies from 5 to 15 eV is almost constant. This means that there are many very energetic O^{2+} produced. This can also be seen in the position and TOF measurement of Straub *et al.* (Fig. 6 in Ref. 6), the O^{2+} shows a very diffuse distribution.

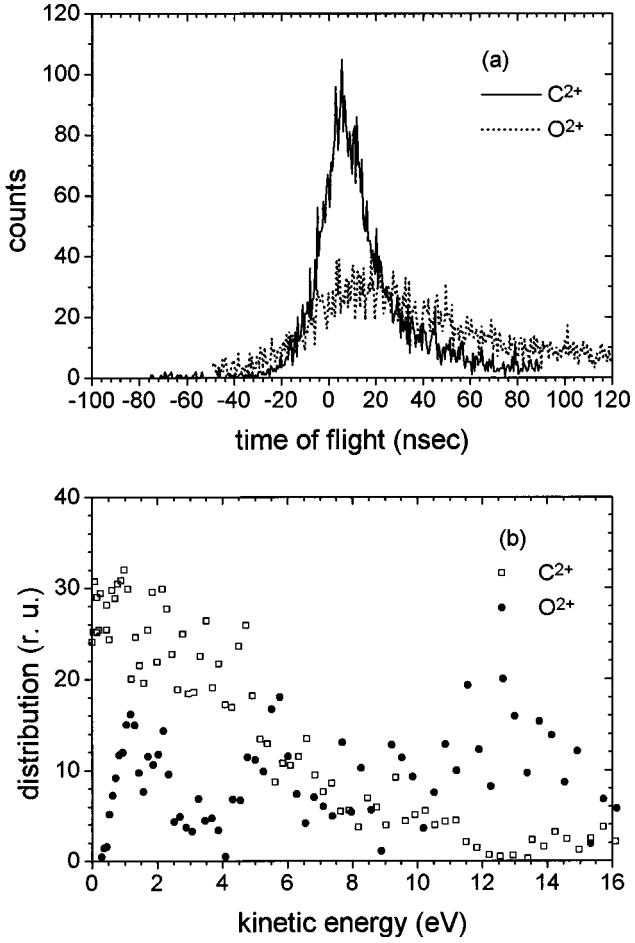

FIG. 16. (a) The TOF profiles of C^{2+} and O^{2+} at the electron energies of 200 eV. The areas of the profiles are normalized to the cross section values. (b) The derived kinetic energy distributions in relative units from the corresponding TOF profiles.

V. DISCUSSION

The measurement of the cross sections for electron impact dissociative ionization has attracted much attention for years. People have been making different efforts to get more reliable data. However, for the measurement of the partial ionization cross sections, satisfactory agreement has been achieved on very few molecules, although all the measurements are generally very carefully calibrated and normalized. This suggests that the error in the measurements are rather systemic than stochastic. Straub *et al.* developed a simple short path TOF mass spectrometer and investigate whether all the ions are collected by observing the local distribution of the ions. They are able to measure the cross sections conclusively.[9,10] The present technique uses a focusing TOF mass spectrometer and estimates the complete collection by deflecting the ion beam and observing the deflection curves. For CO_2 the two techniques agree very well except for some minor discrepancies.

From Figs. 13–15 we see that, among all the singly charged ions, O^+ has a much longer tail at high kinetic energies. This suggests that O^+ is the most difficult ion to be collected completely. This can also be seen in the deflection curves (Fig. 4), the constant collection range of O^+ is much narrower than that of C^+ and CO^+. O^+ has a considerable distribution above 10 eV. These fast ions can hardly be collected by a normal Wiley-McLaren TOF or a quadrupole mass spectrometer. Among all the doubly charged ions, the O^{2+} ions are most energetic. However, the deflection curves suggest the complete collection in the present work. The agreement between our results and those of Straub *et al.*'s confirms the conclusion.

Many measurements were done with a quadrupole mass

spectrometer.[5,21] Generally the cross sections for the parent ions overlap with the present measurements within the error limits. However, for the fragment ions, the disagreement is extremely large. If we compare our results with the quadrupole results of Orient and Srivastava,[5] at an electron energy of 200 eV, our values for CO^+, O^+, and C^+ are 4.15, 3.4, and 5.6 times higher than their values, respectively. These authors stated that they could collect the ions with the kinetic energy of less than 5 eV to the entrance of the quadrupole mass spectrometer. From the measured kinetic energy distribution in the above subsection, the discrepancy between the two measurements should not be so large. The authors calibrated the mass dependent transmission of the quadrupole mass spectrometer.[26] However, the translational energy dependent transmission of the quadrupole mass spectrometer was not considered in the calibration. The translational energy of the fragment ions is dependent on the electron energy, as seen in the last subsection. So the energy dependent transmission of a quadrupole mass spectrometer is very difficult to calibrate, if not impossible. As a result, the quadrupole mass spectrometer tends to just give a relatively accurate result to the ions with a similar kinetic energy distribution to that of the reference ion, which piles up near 0 kinetic energy. The transverse amplitude of the trajectories of the fast fragment ions in the quadrupole mass spectrometer is much bigger. The ions are thus not completely collected. As we see from the kinetic energy measurements, there is a considerable number of O^+ distributed close to 0 kinetic energy. The measurements from the quadrupole mass spectrometer give a relatively big result compared with the case of C^+. There are less C^+ ions distributed close to 0 kinetic energy, so the quadrupole mass spectrometer gives much lower values.

In the present FTOF mass spectrometer, the transmission of the ions is apparently mass independent, since the trajectories of the ions just depend on the initial translational energies and the starting angles. Due to the focusing character the very energetic ions are focused back to the limited effective area of the detector. This allows one to collect all the ions independently of their masses and their initial kinetic energies. The equal collection efficiency to all the ions also allows to measure the initial kinetic energy distribution of the ions. Since the trajectories of the ions are not very far from the axis of the mass spectrometer, the distribution to the kinetic energy is only slightly affected at the high kinetic energy tails.

VI. CONCLUSIONS

A focusing time-of-flight mass spectrometer has been presented for the collection of all the fragment ions from the electron impact dissociative ionization of molecules. Due to the focusing character the ion trajectories are forced close to the axis of the mass spectrometer and are focused back to the effective area of the detector if the ion beam diverges. In the first case we applied the FTOF mass spectrometer to the measurement of the cross sections of the electron impact dissociative ionization of the very important molecule, CO_2. The cross sections have been measured conclusively by observing the deflection curves. The results agree very well with the other conclusive measurements of Straub *et al.*[6] with minor discrepancies. Thus they confirm the results of Straub *et al.* We hope that with this work together with the work of Straub *et al.*, CO_2 becomes one of the few molecules where ''final data'' have been established.

The kinetic energy distributions of the fragment ions have been measured at different electron energies. With the results we analyzed some other previous measurements and explained the big disagreement of the results from the present work. We critically analyzed the technique which made use of a quadrupole mass spectrometer. A quadruple mass spectrometer tends to just collect the slow ions and thus gets much lower values for the fragment ions. Therefore the existing data from quadrupole mass spectrometers on the measurement of the cross section of the electron impact ionization should be rechecked.

ACKNOWLEDGMENTS

One of the authors (C.T.) is grateful to the Alexander von Humboldt Foundation for the financial support for staying at the Max-Planck-Institute for extraterrestrial Physics. Professor S. K. Srivastava is gratefully acknowledged for the encouragement on the design of the time-of-flight mass spectrometer. The technical support of B. Steffes and the stimulating discussions with T. Sykora are also appreciated.

[1] A. L. Hughes and E. Klein, Phys. Rev. **23**, 450 (1924).
[2] K. T. Compton and C. V. Van Voorhis, Phys. Rev. **26**, 436 (1925).
[3] D. Rapp and P. Englander-Golden, J. Chem. Phys. **43**, 1464 (1965).
[4] H. Nishimura and H. Tawara, J. Phys. B **27**, 2063 (1994).
[5] O. J. Orinet and S. K. Srivastava, J. Phys. B **20**, 3923 (1987).
[6] H. C. Straub, B. G. Lindsay, K. A. Smith, and R. F. Stebbings, J. Chem. Phys. **105**, 4015 (1996).
[7] E. Krishnakumar and S. K. Srivastava, J. Phys. B **21**, 1055 (1988).
[8] S-H. Zeng and S. K. Srivastava, J. Phys. B **29**, 3235 (1996).
[9] H. C. Straub, P. Renault, B. G. Lindsay, K. S. Smith, and R. F. Stebbings, Phys. Rev. A **52**, 1115 (1995).
[10] H. C. Straub, P. Renault, B. G. Lindsay, K. S. Smith, and R. F. Stebbings, Phys. Rev. A **54**, 2146 (1996).
[11] H. C. Straub, D. Lin, B. G. Lindsay, K. S. Smith, and R. F. Stebbings, J. Chem. Phys. **106**, 4430 (1997).
[12] C. Tian and C. R. Vidal, Chem. Phys. **222**, 105 (1997).
[13] W. C. Wiley and I. H. McLaren, Rev. Sci. Instrum. **26**, 1150 (1955).
[14] J. L. Franklin, P. M. Hierl, and D. A. Whan, J. Chem. Phys. **47**, 3148 (1967).
[15] F. Esposito, G. Arena, R. Bruzzese, and N. Spinelli, Int. J. Mass Spectrom. Ion Processes **91**, 261 (1989).
[16] G. Arena, V. Berardi, N. Spinelli, R. Velotta, and M. Armenante, Int. J. Mass Spectrom. Ion Processes **127**, 57 (1993).
[17] R. Velotta, P. Di Girolamo, V. Berardi, N. Spinelli, and M. Armenante, J. Phys. B **27**, 2051 (1994).
[18] R. S. Freund, R. C. Wetzel, and R. J. Shul, Phys. Rev. A **41**, 5861 (1990).
[19] E. Krishnakumar, Int. J. Mass Spectrom. Ion Processes **97**, 283 (1990).
[20] T. D. Märk and E. Hille, J. Chem. Phys. **69**, 2492 (1978).
[21] A. Crowe and J. W. McConkey, J. Phys. B **7**, 349 (1974).
[22] B. Adamczyk, A. J. H. Boerboom, and M. Lukasiewicz, Int. J. Mass Spectrom. Ion Processes **9**, 407 (1972).
[23] A. I. Zhukov, A. N. Zavilopulo, A. V. Snegursky, and O. B. Shpenik, J. Phys. B **23**, 2373 (1990).
[24] R. Locht and M. Davister, Int. J. Mass Spectrom. Ion Processes **144**, 105 (1995).
[25] B. Van Zyl and T. M. Stephan, Phys. Rev. A **50**, 3164 (1994).
[26] O. J. Orient and S. K. Srivastava, J. Chem. Phys. **78**, 2949 (1983).